21 October 2022

Molecular Basis for Interferon-mediated Pathogen Restriction in Human Cells

Sumit K. Matta[1], Hinissan P. Kohio[1a], Pallavi Chandra[2a], Adam Brown[3], John G. Doench[3], Jennifer A. Philips[1,2], Siyuan Ding[1], L. David Sibley[1]*

[1]Department of Molecular Microbiology, School of Medicine, Washington University in St. Louis, St Louis. MO 63130

[2]Department of Medicine, Division of Infectious Diseases, School of Medicine, Washington University in St. Louis, St Louis. MO 63130

[3]Broad Institute of Harvard and MIT, Cambridge, MA, 02142

[a] contributed equally

*Correspondence: sibley@wustl.edu

Key words: Interferon gamma, Toxoplasma, Mycobacteria, anti-viral immunity, STAT1, ubiquitin ligase, RNF213, CRISPR/Cas9, genome-wide screen

Abstract

To define novel mechanisms for cellular immunity to the intracellular pathogen *Toxoplasma gondii*, we performed a genome-wide CRISPR loss-of-function screen to provide an unbiased assessment of genes important for IFN-γ-dependent growth restriction. We revealed a previously unknown role for the tumor suppressor NF-2/Merlin for maximum induction of Interferon Stimulated Genes (ISG), which are positively regulated by the transcription factor IRF-1. We then performed an additional focused ISG-targeted CRISPR screen that identified the host E3 ubiquitin ligase RNF213 as essential for IFN-γ mediated control of *T. gondii*. RNF213 mediated ubiquitination of targets on the parasite-containing vacuole and growth restriction in response to IFN-γ in a variety of cell types, thus identifying a conserved factor that plays a prominent role in human cells. Surprisingly, growth inhibition did not require the autophagy protein ATG5, indicating that RNF213 initiates restriction independent of a non-canonical autophagy pathway that has previously been implicated in control of *T. gondii*. RNF213 was also important for control of unrelated intracellular pathogens in human cells treated with IFN, as shown here for *Mycobacterium tuberculosis* and Vesicular Stomatitis Virus. Collectively, our findings establish RNF213 as a critical component of cell-autonomous immunity to a broad spectrum of intracellular pathogens in human cells.

Introduction

Toxoplasma gondii is a widespread parasite of animals that also frequently causes zoonotic infection in humans. As an obligate intracellular parasite, *T. gondii* resides within a specialized vacuole that is largely sequestered from the host endomembrane system (1), which the parasite protects to provide niche for intracellular growth (2, 3). Cell autonomous mechanisms for immune control of intracellular *T. gondii* are best known from studies in the natural murine host, for which laboratory rodents are a useful model (4, 5). Type II interferon, or interferon gamma (IFN-γ), plays the major role in resistance to infection in mouse (6, 7), while type I interferon is also produced and contributes to control of infection (8), particularly in the central nervous system (CNS) during chronic infection (9). Treatment with IFNs leads to upregulation of numerous Interferon Stimulated Genes (ISGs), the exact complement of which varies by cell type (10, 11). Among the most strongly upregulated ISGs are the critically important immunity related GTPases (IRGs) and guanylate binding proteins (GBPs), which collectively lead to vacuole rupture, parasite destruction, and clearance (12-14). The IRG/GBP system is under control of a noncanonical autophagy (ATG) system that requires core ATG components for conjugation of LC3 to phosphatidyl ethanolamine (PE), but it does not require the initiation nor

57 degradative steps (15-17). Although, IRGs and GBPs play a central role in immunity in rodents,
58 human cells largely lack IRGs and GBPs have been described to play a more limited role, as
59 discussed further below.
60 Clinical evidence that human cells control intracellular *T. gondii* via an interferon-mediated
61 process comes from studies demonstrating that immunocompromised patients with low levels of
62 IFN-γ are susceptible to reactivation of latent toxoplasmosis (18, 19). In vitro studies indicate
63 that multiple IFN-γ-dependent pathways can mediate growth restriction in humans. Although
64 humans are not natural hosts in the life cycle, human macrophages are nonetheless able to
65 control the replication of intracellular *T. gondii* in response to IFN-γ (20, 21) and IFN-β (22, 23).
66 Nonhematopoietic human cells also control intracellular *T. gondii* through varied and often cell-
67 type specific mechanisms (24). For example, induction of indole amine oxidase (IDO) by
68 interferon leads to degradation of tryptophan, thus limiting parasite growth in human fibroblasts
69 (25) and human brain microvascular endothelial cells (26). In addition, the noncanonical
70 autophagy pathway described above is required for recruitment of LC3, leading to engulfment of
71 the parasite containing vacuole in multiple membranes, a process that is associated with growth
72 restriction in Hela cells (27), A549 cells (28), and human umbilical vein endothelial cells (29).
73 Curiously, the ATG-dependent growth restriction is not global (16), but rather limited to those
74 vacuoles that become ubiquitinated and acquire adaptors such as p62, NDP52, and LC3 (27,
75 29). Virulent type I strains are largely resistant to this pathway, while types II and III are
76 susceptible (27), although the basis for this difference is unknown. Recent studies identified the
77 E3 ubiquitin ligase RNF213 as a candidate for mediating early ubiquitination of *T. gondii*-
78 containing vacuoles in IFN-γ treated A549 cells (30). The IFN-γ signaling and noncanonical ATG
79 pathways are partially connected by ISG15, which is required for maximal recruitment of ATG
80 adaptors and also interacts with RNF213 (28). Additionally, GBP1 has been implicated in
81 restricting *T. gondii* growth in human epithelial cells, despite not being recruited to the vacuole
82 (31), while it is recruited to the vacuole membrane in THP-1 cells, resulting in rupture and
83 activation of apoptosis (32). Additionally GBP2 and GBP5 contribute to growth restriction in
84 THP-1 cells, despite not being recruited to the parasite containing vacuole (33). Collectively,
85 these prior candidate-gene studies indicate that multiple IFN-γ–dependent mechanisms can
86 contribute to growth restriction, which is often partial and expressed in a cell-specific manner.
87 However, the absence of any prior global or unbiased assessment of genes required for IFN-γ
88 mediated growth restriction leaves open the possibility that a previously unrecognized, IFN-γ-
89 mediated pathway exists in all or most human cells.

90 To provide an unbiased assessment of the predominate pathways for control of *T. gondii*
91 growth in IFN-γ activated human cells, we performed genome-wide CRISPR screen in A549
92 cells. Our findings reveal a previously unanticipated role for the tumor suppressor NF2 in
93 modulating IRF-1-dependent gene expression, hence dampening ISG expression. Additionally,
94 an ISG-focused CRISPR screen identified the E3 ligase RNF213 as an essential component of
95 control of *T. gondii* in multiple human cell lines treated with IFN-γ. Surprising, although RNF213
96 was associated with ubiquitination and recruitment of ATG adaptors including LC3, it functioned
97 independently of the previously described pathway for non-canonical autophagy. Moreover,
98 RNF213 exerted a general antimicrobial activity against intracellular bacteria and viruses,
99 including *Mycobacterium tuberculosis* and vesicular stomatitis virus, revealing a conserved role
100 in cell autonomous immunity in human cells.
101

102 ## Results

103 **Genome-wide CRISPR screen identifies factors important for IFN-γ mediated growth**
104 **restriction**

105 Although depletion of tryptophan due to induction of IDO has been described as a mechanism
106 for restricting growth of *T. gondii* in some cell types (24), we previously reported that disruption
107 of the IDO gene in A549 cells has no impact on IFN-γ mediated growth restriction (34).
108 Consequently, we selected A549 cells to define novel mechanisms for IFN-γ mediate growth
109 restriction based on CRISPR-mediated loss of function screens. Initially, we validated the
110 growth restriction following IFN-γ activation of A549 cells using a previously described vacuole
111 size assay (9). We used the type III strain named CTG of *T. gondii* as it is highly susceptible to
112 growth restriction, relative to either type I or type II strains (27, 35). The vacuole size assay
113 takes advantage of the fact that parasite replication leads to increased size of the vacuole while
114 growth inhibition by IFN-γ blunts the expansion of parasites. Quantification of vacuole size after
115 IFN-γ treatment verified that wild type (WT) cells restricted parasite expansion and that this
116 ability was IFN-γ dependent, as shown by loss of growth restriction in STAT1 knockout (STAT1-
117 KO) cells (**Fig. 1A, Fig. S1A**). As expected, the growth restriction was independent of
118 exogenously added tryptophan, indicating it does not rely on IDO1, even though this gene is
119 induced in IFN-γ treated A549 cells (34). To develop a process for selecting cells from the
120 population, we infected A549 cells with a recombinant CTG strain expressing GFP (CTG-GFP),
121 trypsinized cells from the dish, and analyzed them by flow cytometry to evaluate the average
122 intensity of GFP as a proxy for parasite growth (**Fig. 1B**). Although there was not a distinct

separation between the populations of CTG-GFP in WT vs. STAT1-KO cells, there was a clear shoulder of higher GFP expression in the STAT1-KO cells (green box, **Fig. 1B**). We therefore reasoned that escape mutants that lose the ability to control parasite replication should mimic the growth of CTG-GFP in STAT1-KO cells, thus providing the basis for the CRISPR-based screens described below.

We then used lentiviral transduction of A549 cells to express the Brunello library containing 4 guides each to ~20,000 genes in the human genome (36) and developed a screen for loss of IFN-γ mediate growth restriction (**Fig. 1C**). We scaled the culture assays to aim for single sgRNA per cell with ~ 100x coverage of each gene such that loss of guides during expansion could be quantified. Cells were expanded for 8 passages to allow for stabilization of the population of guides that did not affect viability. Cells were then activated with IFN-γ, infected with CTG-GFP, and the top 5% of GFP expressing cells were sorted from four independent experiments (**Fig. 1D**). The sgRNAs from these pools were amplified, barcoded, and subjected to NGS sequencing using the Illumina platform. We reasoned that sgRNAs that are enriched in the top 5% pool represent genes whose loss results in impaired IFN-γ mediated growth restriction of CTG-GFP. Comparison of the guide abundances in the top 5% relative to a time-matched point for the uninfected pool was used to classify guides that were significantly different based on Fold Change and FDR (False Discovery Rate) in the four replicates of the primary screen (**Fig. 1E**, **Dataset 1**). There was a high degree of variability in genes that were scored significant between the various replicates. For example, only 5 genes (including NF2, FRYL) met the individual *P* value for significance in all 4 replicates when analyzed separately (**Fig. S1B**). Additionally, 23 genes were individually significant in 3 of 4 while 224 were significant in 2 of 4 replicates (**Fig. S1B**). However, using the more stringent criteria of FDR for the combined replicates, only NF2 and FRYL were scored as significant (**Fig. 1E**). Although guides for STAT1 and IRF1 were slightly enriched, the strongest signal for enhanced sgRNA guides correspond the gene NF2 (Neurofibromatosis 2) an Ezrin / Radixin / Moesin (ERM) family member that is also known as MERLIN (37), and which functions as a tumor suppressor (**Fig. 1E**). We also detected three genes that showed depletion of sgRNAs (PTEN, TSC1 and TSC2) (**Fig. 1E**). Although we have not followed up on these hits, they presumably are depleted because cells lacking these genes have decreased survival during infection and IFN-γ treatment.

Secondary pool CRISPR screen identifies IFN-γ-STAT1 axis and NF2 as critical for growth restriction

156 Comparison of the results from the primary screen revealed a high degree of variability in
157 genes classified as significantly different between the replicates, which is not unexpected for
158 FACS-based screens (38). We therefore considered it possible that the genome-wide screen
159 may have missed genes that contribute to IFN-γ mediated resistance. Consequently, we
160 developed a secondary screen based on a pool of genes that were significantly enriched in at
161 least 2 of 4 replicates of the primary screen (**Fig. S1B**). The secondary screen included 224
162 genes with coverage of 10 sgRNAs per gene, thus improving statistical power for identifying
163 differences. The secondary screen identified several factors in the IFN-γ-STAT1 axis; their loss
164 suggests that they are essential for growth restriction **(Fig. 1F**) (**Dataset 2**). Included in the set
165 of highly enriched guides representing depleted genes were STAT1, the JAK2 kinase that
166 phosphorylates STAT1, the IFN-γ receptor subunits IFNGR1 and IFNGR2 as well as the
167 downstream transcription factor IRF-1, which augments the activity of IFN-γ on inducing gene
168 expression (39) (**Fig. 1F**). The only gene not part of the IFN-γ-STAT1 pathway was NF2, which
169 was the top hit in the primary screen (**Fig. 1F**). The four other genes that were significantly
170 enriched in each replicate of primary screen, including FRYL, were not enriched in the T5
171 population of the secondary screen.
172 NF2 has previously been implicated in suppressing tumors via interaction with the E3
173 ubiquitin ligase CRL4 in the nucleus (37), and in regulating mTOR (40) and modulating
174 metabolism (41); however, it has not previously been associated with IFN-γ activation nor
175 pathogen control. To elucidate its contribution to cell-autonomous pathogen control, we
176 generated KOs using lentiviral transduction and targeted CRISPR-Cas9 gene editing for both
177 NF2 and IRF-1 in A549 cells (**Fig. S2**). As expected, IRF-1 showed dependence for expression
178 in WT cells and NF2-KO cells on IFN-γ treatment, while NF2 was not affected by IFN-γ
179 treatment (**Fig. 2A**). We then ascertained the ability of IFN-γ to control growth of CTG parasites
180 in WT, IRF-1 KO and NF2 KO cells using the vacuole size assay. As expected, growth
181 restriction seen in WT cells was completely lost in IRF-1 KO cells, consistent with previous
182 reports that this transcription factor is essential for control of *T. gondii* in IFN-γ treated cells (34).
183 In contrast, loss of NF2 resulted in a partial, yet significant reduction in the growth restriction
184 following IFN-γ (**Fig. 2B and 2C**).
185 **Loss of NF2 down-modulates IRF-1 dependent ISG expression**
186 To better define the role of NF2 in IFN-γ dependent growth restriction, we compared the
187 transcriptional profile of WT, IRF-1 KO and NF2 KO cells under resting and activated conditions.
188 Comparison of the NF2 KO to WT cells revealed multiple of genes that were NF2 dependent

189 (**Fig. S3**), which likely reflect its diverse roles. However, when we compared the IFN-γ induced
190 genes that were IRF-1-dependent, there was a clear pattern that most of these genes were also
191 dampened in the NF2 KO (**Fig. 2D**). The extent of suppression in the NF2 KO varied among
192 genes: for example, APOL3 was IRF-1 dependent but only partially affected by NF2, whereas
193 IDO, GBP4 and RARES3 were more strongly affected by NF2 as well as IRF-1 (**Fig. 2E**). We
194 also examined the effect of NF2 on IFN-β driven expression using an ISRE (Interferon
195 Stimulation Response Element) promoter normalized to constitutively expressed firefly
196 luciferase. Induction of ISRE activity by IFN-β was significantly lost in both IRF1 KO and NF2
197 KO cells (**Fig. 2F**), indicating that both factors likely also participate in IRF-1 mediated
198 transcription.

199 **ISG targeted CRISPR screen identifies RNF213 as the primary determinant of IFN-γ**
200 **mediated growth restriction in multiple human cell types**

201 We were surprised that neither the primary nor secondary genome-wide screens identified
202 any canonical ISGs, except for the broadly acting transcription factor IRF-1, which affects many
203 ISGs. Consequently, we designed a focused CRISPR screen based on a previous set of ISGs
204 that was defined by transcriptional induction in response to IFN-γ in A549 cells (34). The ISG
205 screen included ~350 genes with coverage at 10 sgRNAs per gene and was repeated four
206 times independently (**Fig. 3A**). Sequencing the top 5% of CTG-GFP positive cells was used to
207 define sgRNAs that were significantly enriched, thus identifying genes important for IFN-γ
208 mediated control. We identified only a single strong positive corresponding the E3 ligase
209 RNF213, in addition to the broadly acting IRF-1 (**Fig. 3B**) (**Dataset 3**). RNF213 is not widely
210 recognized as an ISG due to its constitutive expression in many cell types, and yet it is
211 upregulated by ~ 8 fold in A549 cells treated with IFN-γ and thus was part of the library used in
212 the screen. RNF213 ranked 304 in the primary screen (**Dataset 1**) but did not meet the criteria
213 for the secondary pool screen, although sgRNA guides for this gene were enriched in the top
214 5% population in 3 of 4 replicates by > 2 fold. Given its prominent position in the targeted ISG
215 screen, we decided to examine its function. Deletion of RNF213 resulted in enhanced growth of
216 CTG strain parasite in both untreated cells and it completely reversed the growth inhibition
217 normally seen in IFN-γ treated A549 cells (**Fig. 3C and 3D**). Notably, although sgRNAs were
218 present for IDO1, ISG15, GBP1, and RARRES3, their frequency was not changed in the top 5%
219 pool, indicating the singular loss of these genes does not contribute substantially to IFN-γ
220 mediated growth restriction under the conditions of the screen.

221 Many factors that have been previously described to restrict *T. gondii* growth in IFN-γ treated
222 human cells are either cell type specific or limited to specific parasite lineages (24). To test how
223 widely conserved the function of RNF213 was, we generated KOs in human foreskin fibroblasts
224 (HFF) and in the human monocytic cell line THP-1 (**Fig. S4**). Similar to the situation in A549
225 cells, loss of RNF213 resulted in slightly enhanced growth in untreated HFF cells and a loss of
226 IFN-γ mediated growth inhibition (**Fig. 3E and F**). Additionally, the loss of RNF213 in THP-1
227 cells reversed the inhibition of *T. gondii* growth following treatment with either IFN-γ or IFN-β
228 combined with TNF-α (**Fig. 3G and H**). Notably, the loss of RNF213 in all three cell types
229 completely reversed the effects of IFN-γ, similar to loss of STAT1 or IRF-1 in A549 cells.
230 Additionally, the expression of RNF213 was sub-maximal in IRF-1 KO and NF2 KO cells treated
231 with IFN-g (**Fig. S4A**), suggesting they may act through this downstream mediator. Collectively,
232 these findings argue that RNF213 is the major effector downstream of both type I and type II
233 IFNs that inhibits parasite growth in human cells.

234 **RNF213-dependent growth restriction leads to recruitment of autophagy adaptors but is**
235 **independent of ATG5**

236 Consistent with its requirement for growth restriction, RNF213 was recruited to a portion of
237 *T. gondii* vacuoles in untreated cells, and this increased dramatically following treatment with
238 IFN-γ as shown by immunofluorescence assay (IFA) and immuno-EM (**Fig. 4A-C**). Since
239 ubiquitination is thought to be the first step in marking the *T. gondii* vacuole for growth restriction
240 (27), we stained cells with FK2, which recognizes both mono and poly ubiquitin (Ub) chains, in
241 combination with RNF213. The proportion of vacuoles that were FK2 positive closely matched
242 the percentage that were also positive for RNF213, while the number that were RNF213 positive
243 considerably exceeded this value (**Fig. 4C**). The higher percentage of RNF213 positive staining
244 vacuoles, suggesting that RNF213 is initially recruited to the PVM followed by ubiquitination,
245 resulting in double positive vacuoles. Similar co-staining of RNF213 and FK2 was observed in
246 IFN-γ activated HFF and THP-1 cells infected with CTG (**Fig. S5).** Downstream of IFN-γ
247 mediated ubiquitination, the PVM acquires several adaptors, including p62 and NDP52, that
248 recruit the autophagy adaptor LC3 (27-29). Consistent with these previous reports, recruitment
249 of LC3 was low in non-activated cells, and significantly elevated after treatment with IFN-γ (**Fig.**
250 **4D and E**). The proportion of vacuoles that were positive for both FK2 and LC3 was similar,
251 while singly FK2 positive vacuoles considerably exceeded this value (**Fig. 4E**). These
252 differences in positivity suggests that ubiquitination occurs first, followed by recruitment of LC3.

253 Examination of the vacuole membrane surrounding the parasite by TEM revealed that it was
254 often wrapped by numerous membranes (**Fig. 4F**), a phenotype that has previously been
255 associated with growth restriction by non-canonical autophagy (27). Combined with the
256 recruitment LC3, this profile suggested that RNF213 may act to recruit components of the non-
257 canonical autophagy pathway to restriction growth of the parasite. To test this idea, we
258 generated a knockout of ATG5 in A549 cells, and verified its absence by western blotting and
259 loss of conversion of LC3I to the lipidated LC3II form (**Fig. 4G**). Contrary to expectation, loss of
260 ATG5 minimally affected the growth restriction of *T. gondii* in IFN-γ treated cells (**Fig. 4H**). To
261 ascertain whether loss of ATG5 might have affected the recruitment of RNF213 to the parasite
262 containing vacuole, we stained IFN-γ treated and infected ATG5 KO cells for RNF213 and FK2.
263 Similar to WT cells, parasites were frequently labeled by both RNF213 and FK2 in ATG5 KO
264 cells (**Fig. 4I**). Collectively, these findings indicate that RNF213 lies upstream of ubiquitination
265 and that growth restriction requires RNF213 but not an ATG5 dependent process.
266
267 **RNF213 participates in interferon-mediated control of bacterial and viral pathogens**
268 Previous studies have described a role for RNF213 in recognition and ubiquitination of LPS on
269 intracellular *Salmonella* (42). To explore the role of RNF213 in control of intracellular bacteria
270 that do not contain LPS, we examined the requirement for RNF213 in IFN-γ activated A549 cells
271 infected with *Mycobacterium tuberculosis* (Mtb). Human cells normally are not able to clear
272 intracellular Mtb following treatment with IFN-γ but rather restrict their intracellular growth.
273 Consistent with this profile, the colony forming units of Mtb remained static in IFN-γ treated cells
274 grown for 48 h, compared to control cells where they increased significantly (**Fig. 5A**). Loss of
275 RNF213 significantly impaired the ability of IFN-γ to control replication of Mtb (**Fig. 5A**).
276 Immunofluorescence localization also revealed that RNF213 was recruited to the surface of Mtb
277 in A549 cells and that these vacuoles also stained with FK2 indicating that they were
278 ubiquitinated (**Fig. 5B**). RNF213 has also been reported to facilitate control of Rift Valley fever
279 virus, an enveloped segmented RNA virus (43). We also explored the potentially broad anti-
280 microbial role of RNF213 in control of intracellular viral replication using a non-segmented RNA
281 virus. We examined type I IFN (IFN-β) treated A549 cells infected with vesicular stomatitis virus
282 expressing GFP (VSV-GFP). Treatment with IFN-β resulted in a significant decrease in viral
283 replication in WT cells that was reversed in IRF-1 KO and RNF213 KO cells (**Fig. 5C and D**).
284 Collectively, these findings suggest that RNF213 may recognize a host component that is

common to multiple pathogens, rather than a panoply of different molecules each unique to one pathogen.

Discussion

To identify conserved mechanisms of cell autonomous immunity to intracellular pathogens, we performed a genome-wide CRISPR screen for loss of *T. gondii* growth restriction in response to IFN-γ. Although the primary screen failed to identify previous candidate genes implicated in control, we ascribed a new role for the tumor suppressor gene NF2 in upregulating expression of IRF-1 dependent ISGs. To account for the possibility that the primary screen lacked power to identify single gene effects, we performed an ISG-targeted screen for loss of IFN-γ-mediated *T. gondii* growth restriction. The ISG-targeted screen identified the E3 ligase RNF213 as the primary effector important for IFN-γ mediated control of *T. gondii* growth in human cells. RNF213 was upregulated by IFN-γ, recruited to the parasite containing vacuole, and associated with initial ubiquitination of targets at this interface. Deletion of RNF213 revealed that it was necessary for growth restriction, despite not relying on ATG5, which may act at downstream steps independent of growth restriction. Loss of RNF213 also diminished antibacterial and antiviral responses to interferon, suggesting it controls a common host pathway needed for pathogen resistance. These studies define a broad role for RNF213 as an essential mediator of growth restriction of divergent pathogens in a variety of human cell types.

Although previous studies have focused on candidate genes, we were interested in an unbiased method to identify genes important for IFN-γ mediated control of *T. gondii*. To this end, we developed a FACS-based CRISPR-screen to identify genes whose absence results in loss of IFN-γ mediated growth restriction of a GFP-expressing strain of *T. gondii*. The genome-wide CRISPR screen identified a number of components in the STAT1 signaling pathway including JAK2, the receptors IFNGR1 and IFNGR2, and the transcription factor IRF-1. These hits validate the screen as being sufficient to identify factors that globally affect the IFN-γ response. In particular, IRF-1 amplifies the responses normally triggered by engagement of STAT1 on promoters bearing GAS sequences (44), thus upregulating a constellation of ISGs. Consistent, with this ability we found that IRF-1 was necessary for maximal growth control following IFN-γ stimulation. Independently, we have previously shown that overexpression of IRF-1 in A549 cells is sufficient to induce control of *T. gondii* growth (34). We also identified NF2 as a significant hit in the primary genome-wide and pooled secondary CRISPR screens. Consistent with its prominent ranking in the CRISPR screens, deletion of NF2/Merlin significantly reduced the expression of IRF-1-dependent genes ungulated by IFN-γ, in addition to dysregulating

319 numerous unrelated genes. This finding was unexpected as NF2 is known as a tumor
320 suppressor gene that negatively regulates mTOR and the Hippo signaling pathways but is
321 without prior connection to interferon signaling (40, 41). NF2/Merlin binds to and inhibits the E3
322 ubiquitin ligase CRL4 in the nucleus, thereby suppressing tumorigenesis (37). Previous studies
323 have shown that CRL4 ubiquitinate histones and/or transcription factors leading to down-
324 regulated gene expression (45). Hence, it is possible that in the absence of NF2/Merlin, CRL4
325 may target IRF1 to down-regulate its activity. Among the ISGs that are NF2 and IRF-1
326 dependent, RNF213 may factor prominently given its essential downstream role in mediating
327 IFN-γ growth inhibition.
328 Because the genome-wide CRISPR screen failed to find previous candidate genes, we
329 considered it might lack sufficient power to identify such single factors. As such, we performed a
330 targeted CRISPR screen of ISGs that we have previously shown to be upregulated in A549 cells
331 (34). Despite the fact that this screen included a number of previously recognized factors that
332 control IFN-γ mediated growth in other human cells including RARES3 (34), ISG15 (28), GBPs
333 (32, 33), and IDO (25), these genes were not identified as significant hits. This finding suggests
334 that while these genes have demonstrable effects when tested individually, their individual
335 contributions are too modest to show differences at the population level, at least based on the
336 conditions used here. Instead of these previously characterized factors, the ISG-targeted
337 CRISPR screen identified a prominent role for RNF213, which is expressed at basal levels and
338 upregulated in response to IFN-γ (34). RNF213 was essential for IFN-γ mediated restriction of *T.*
339 *gondii* growth in multiple human cell types. We previously shown that type I IFN also restricts *T.*
340 *gondii* growth in human THP-1 macrophages (3) and we now show that this restriction is
341 downstream of RNF213.
342 We observed that RNF213 was recruited to a proportion of parasite containing vacuoles
343 even in unstimulated cells, consistent with the fact that it is expressed at basal levels yet
344 induced by IFN-γ. Similarly, RNF213 has been shown to be recruited to vacuoles containing
345 intracellular *Salmonella* (42), *Listeria* (46), and *Chlamydia* lacking the effector GarD (47), and to
346 restrict their growth in the absence of IFN-γ stimulation. We observed a slight increase in the
347 growth of *T. gondii* in non-stimulated cells lacking RNF213; however, the major role for this
348 factor was in IFN-γ treated cells which completely lost growth inhibition in the absence of
349 RNF213. Notably, RNF213 was recruited early during infection and was associated with
350 ubiquitination of targets on the parasite containing vacuole. It was also present there before
351 autophagy marker LC3 and notably its presence on the vacuole did not rely on ATG5.
352 Moreover, the growth restriction imparted by IFN-γ treatment was largely independent of ATG5

353 and yet fully dependent on RNF213. Taken together, these finding suggest a model whereby
354 RNF213 is initially recruited to the parasite-containing vacuole where it ubiquitinates unknown
355 targets leading to growth restriction, followed by recruitment of a non-canonical ATG pathway,
356 which while not required for growth restriction may be important in downstream events.
357 The mechanism by which RNF213 is recruited to pathogen containing vacuoles remains
358 undefined, but the broad specificity of this pathway suggests that there may be some common
359 determinant recognized by the multiple domain structure of RNF213 that includes a dynein-like
360 core with 6 ATPase units and a multi-domain E3 module (48). Similarly, the targets of
361 ubiquitination on other pathogen-containing vacuoles remain undefined. Previous studies have
362 suggested LPS on cytoplasmically exposed *Salmonella* is targeted by ubiquitination (42),
363 although the exact chemical adduct remains to be defined. However, other pathogens including
364 intracellular *Listeria*, and various viruses that have been shown to be targeted by RNF213 (46),
365 lack LPS. The pathogens studied here also do not contain LPS, indicating that they must be
366 recognized by a different mechanism. The broad nature of organisms targeted by RNF213
367 favors a model in which RNF213 recognizes a host target, either protein or lipid, whose
368 modification leads to restricted pathogen growth. Future studies to elucidate this mechanism
369 may enable enhanced cell-autonomous immunity to clear intracellular pathogens without the
370 adverse effects of treatment with interferons.
371

372 **Acknowledgements**

373 We thank Dr. Wandy Beatty, Microbiology Imaging Facility, Washington University in St. Louis
374 for performing the electron microscopy studies. We also thank Jennifer Barks for cell culture
375 support, members of the Sibley lab for helpful comments, Robert Orchard for advice on the
376 CRISPR screens, and Felix Randow for communications prior to publication. This work was
377 presented prior to publication at the Woods Hole Immunoparasitology Meeting (April 10-13,
378 2022) and the 16th International Congress on Toxoplasmosis (May 22-26, 2022). Supported in
379 part by grants from the NIH (AI154048, AI118426).
380

381 **Author contributions**

382 Conceptualization: SKM, LDS; Data curation, SKM; Investigation; SKM, HPK, PC; Formal
383 Analysis, SKM, HPK, PC; Methodology: AB, JD; Project administration and supervision, JAP,
384 SD, LDS; Visualization SKM, HPK, PC; Writing, SKM, SD, JAP, LDS.
385

386 **Database submission**

387 RNASeq data have been submitted to GEO under the accession number GSE215771 and will
388 be made available to reviewers and released prior to publication.
389
390 ## Supplementary Materials
391
392 **Fig. S1A Validation of STAT1 knockout A549 line.**
393 **Fig. S1B Comparison of top hits for four primary CRISPR screens.**
394 **Fig. S2 Validation of IRF-1 and NF2 knockouts in A549 cells.**
395 **Fig. S3 Summary of NF2 dependent genes based on RNASeq.**
396 **Fig. S4 Validation of RNF213 knockouts in HFF and THP-1 cells.**
397 **Fig. S5 IFA staining of RNF213 and ubiquitination in CTG infected IFN-γ activated HFF**
398 **and THP-1 cells.**
399 **Table S1 Primers used for sgRNA cloning**
400 **Dataset 1 Results of four primary CRISPR screens.**
401 **Dataset 2 Results of pooled secondary CRISPR screens.**
402 **Dataset 3 Results of ISG targeted CRISPR screens.**
403
404 ## Materials and Methods
405 ### Reagents and antibodies
406 Rabbit polyclonal anti-RNF213 (#HPA003347), Tryptophan, puromycin, polybrene and phorbol
407 12-myristate 13-acetate (PMA) were obtained from Sigma-Aldrich (St. Louis, MO, USA). Human
408 IFN-γ, human TNF-α and human IFN-β were obtained from R&D systems (Minneapolis, MN,
409 USA). *T. gondii* parasites were stained with mouse mAb DG52 against the surface antigen
410 SAG1 (49) and GRA7 was detected using a rabbit polyclonal serum described previously (50).
411 Mouse monoclonal anti-polyubiquitin (FK2, # 04-0263) antibody was obtained from Millipore
412 Sigma Life Sciences. Rabbit mAb anti-IRF1 (D5E4, # 8478) and rabbit mAb anti-STAT1 (D1K9Y
413 #14994) were obtained from Cell Signaling Technologies. Rabbit polyclonal LC3 (# PM036) was
414 obtained from MBL International Corporation. Rabbit polyclonal anti-NF2 (ab217016) antibody
415 was obtained from Abcam. Mouse monoclonal anti-ATG5 (#66744-1-Ig) was obtained from
416 Proteintech Group, Inc. Secondary anti-IgGs conjugated to IRDye800 and IRDye700 were
417 obtained from Li-Cor Biosciences (Lincoln, NE, USA). Hoechst, goat anti-mouse IgG and goat
418 anti-rabbit IgG secondary antibodies conjugated to Alexa 488 or Alexa 594, were obtained from
419 Life technologies Corporations (Grand Island, NY, USA). Secondary anti-IgG conjugated to 18

420 nm gold particle in immuno-electron microscopy was obtained from Jackson ImmunoResearch
421 Laboratories, Inc., (West Grove, PA).
422

423 **Parasite and mammalian culture**

424 Type III CTG expressing GFP parasites were generated previously (34). Parasites were grown
425 as tachyzoites in human foreskin fibroblasts (HFF) obtained from the laboratory of Dr. John
426 Boothroyd, Stanford University, as described previously (9). Parasites were harvested shortly
427 after natural egress and purified by passage through 20 g needle and separated from host cell
428 debris using 3.0 micron polycarbonate filters (Whatman). HFFs, HEK-293T and A549 lung
429 epithelial carcinoma cells were maintained in DMEM with 10% v/v FBS at 5% CO_2 and 37 ^{0}C.
430 THP-1 human monocytic cells were maintained in RPMI with 10% v/v FBS at 5% CO_2 and 37
431 ^{0}C. THP-1 cells were first differentiated into macrophages with 50 nM PMA for 48 h. PMA was
432 washed off and cells were further incubated in their maintenance media for 24 h before use. All
433 strains and host cell lines were determined to be mycoplasma-negative using the e-Myco Plus
434 Kit (Intron Biotechnology).

435 **Lentiviral transduction of the Brunello library**

436 The Brunello library (# 73179) expressing 76,441 sgRNAs against 19,114 human genes + 1,000
437 non-targeting sgRNA controls in plentiCRISPRv2 was obtained from Addgene (51). The library
438 was electroporated into Endura electrocompetent cells (# 60242; Lucigen Bioresearch
439 Technologies) and plasmid was prepared from > 80 million bacterial colonies (>1,000X
440 representation). Briefly, twenty-five 60 mm tissue culture dishes, each containing 2.6 million
441 293T cells, were plated 24 h prior to transfection. A combination of 15 μg of plentiCRISPRv2
442 harboring the Brunello library, 5μg of pRSV-Rev (Addgene # 12253), 7 μg of pMD2.G (Addgene
443 # 12259), and 11 μg of pMDLg/pRRE (Addgene # 12251) were co-transfected per tissue culture
444 dish using Lipofectamine LTX reagent with PLUS reagent (Thermo Fisher Scientific) as per
445 manufacturer's instruction. The supernatant of 293T cells was collected 72 h after transfection
446 and filtered using 0.45 μm PES filter. A total of ten 150 mm tissue culture dishes, each
447 containing 10 million A549 cells, were seeded 24 h prior to virus transduction. The virus in the
448 supernatant was serially diluted and transduced into A549 cells using polybrene (8 ug/ml) to
449 achieve ~ 10% transduction efficiency. The media was changed 72 h after transduction and
450 cells were selected with 4 μg/ml of puromycin. In parallel, 800,000 A549 cells per well were
451 seeded in 6-well plates to calculate the coverage of transduced Brunello library. Transduced
452 coverage was calculated by measuring percent survival of virus transduced cells 72 h after

453 incubation with 4 μg/ml puromycin relative to untreated control. The cells were selected on 4
454 μg/ml puromycin for two weeks to select the transduced cells. The Brunello library transduced
455 A549 cells were passage 8 times before their use in the FACS based experiments. The library
456 transduced cells were always spilt at a minimum of 100X coverage or 7.5 million cells in new
457 T350 cm^2 tissue culture flasks for every passage until completion of the experiment.

458 **Cloning of secondary sgRNA CRISPR library**

459 Secondary screen: sgRNAs of genes that were significantly enriched (log2Fold Change > 1 and
460 $P < 0.05$) in T5 over uninfected control in 2 out of 4 replicates of the primary Brunello library
461 screens were selected to conduct a secondary screen. Ten sgRNAs per gene against 224
462 selected genes were designed using sgRNA designer at the Genetic Perturbation Platform
463 (GPP) web portal (https://portals.broadinstitute.org/gpp/public/analysis-tools/sgrna-design).
464 Additionally, 260 negative control sgRNAs were randomly selected from 1,000 negative control
465 sgRNAs in the Brunello library with 130 each corresponding to NO_SITE and
466 ONE_INTERGENIC_SITE negative controls. The oligonucleotide library was synthesized at
467 Genescript. Briefly, the 20 bp sgRNAs in the library were flanked by complementary sequences
468 in the plentiCRISPRv2 vector with CTTGTGGAAAGGACGAAACACCG oligonucleotide at the 5'
469 end and GTTTTAGAGCTAGAAATAGCAAGTTAAAATAAGGC at the 3' end. The library was
470 PCR amplified and Gibson cloned (52) into BsmBI digested plentiCRISPRv2. Assembled
471 plasmid was dialyzed on a Type-VS Millipore membrane (MF type, VS filter, mean pore size =
472 0.025 μm, Millipore, Inc. #VSWP 02500) and electroporated into Endura electrocompetent cells.
473 A549 cells were transduced with the secondary pool library at > 100X coverage, as described
474 above, and selected with 4 μg/ml puromycin for two weeks. The secondary library transduced
475 cells were passage 8 times before their use in the FACS based experiments and were always
476 spilt at a minimum of 100X coverage for every passage until completion of the experiment.
477

478 **Cloning of the Interferon Stimulated Gene (ISG) sgRNA library**

479 Genes that are significantly induced in A549 cells upon IFN-γ stimulation (34) were selected for
480 sgRNA design. Ten sgRNA per gene were designed for 352 ISGs using the GPP web portal. A
481 total of 480 negative control sgRNAs were randomly selected from 1,000 negative control
482 sgRNAs from the Brunello library with 240 each corresponding to NO_SITE and
483 ONE_INTERGENIC_SITE negative controls. The oligonucleotide library was synthesized at
484 Genescript. The 20 bp sgRNAs in this library were flanked by BsmBI recognition sites along with
485 overhang sequence for ligation with BsmBI digested plentiCRISPRv2. The 79 oligonucleotide

486 library consists of 20 bp sgRNA sequences flanked with 5'
487 GCACTTGCTCGTACGACGCGTCTCACACCG sequence and 3'
488 GTTTCGAGACGTTAAGGTGCCGGGCCCAC sequence. The library was PCR amplified,
489 digested with BsmBI, and ligated into plentiCRISPRv2 using NEB Golden Gate Assembly Kit
490 (BsmBI-v2) (New England Biolabs Inc. # E1602S). The ligation reaction was dialyzed on a
491 Type-VS Millipore membrane and electroporated into Endura electrocompetent cells. A549 cells
492 were transduced with the ISG library at > 100X coverage, as described above and selected on 4
493 μg/ml puromycin for two weeks. The ISG library transduced cells were passage 8 times before
494 their use in the FACS based experiments and were always spilt at a minimum of 100X coverage
495 for every passage until completion of the experiment.

496 **Flow cytometry and cell sorting**

497 Wild type and STAT1 knockout (STAT1 KO) A549 cells were cultured ± 100 U/ml IFN-γ for 24 h
498 prior followed by washing with complete media. The cells were infected with CTG expressing
499 GFP (CTG-GFP) at MOI 0.5 and cultured for 40 h. Cells were washed, trypsinized, and fixed
500 with 4% paraformaldehyde followed by analysis on Sony SH800S cell sorter. Single cells were
501 gated and GFP fluorescence was used to monitor intracellular growth of CTG-GFP. FACS-
502 based CRISPR screens were executed by pre-activating 30-50 million library transduced A549
503 cells with 100 U/ml of IFN-γ for 24 h. The cells were washed and infected with CTG-GFP at MOI
504 0.5 and incubated for 40 h. Cells were washed, trypsinized, and filtered (40 μm) prior to sorting.
505 Single cells were gated and top 5% of events (T5) based on GFP fluorescence intensity were
506 sorted. Genomic DNA was isolated from the top 5% CTG-GFP infected cells and uninfected
507 cells for each of 4 biological replicates for each library. Uninfected control cells for each
508 replicate were passage matched with the sorted T5 population.

509 **Genomic DNA isolation and next generation sequencing**

510 Genomic DNA was isolated using Qiagen DNeasy kit as per manufacturer's instructions. PCR
511 was done using Ex Taq in a 100 μl reaction with the maximum of 10 μg of template per reaction
512 (36). The amplicons for next generation sequencing were generated using a 2-step PCR
513 amplification of integrated sgRNAs. Briefly, genomic DNA isolated from different samples was
514 used as template for PCR1 using forward 5'
515 TCGTCGGCAGCGTCAGATGTGTATAAGAGACAGGGCTTTATATATCTTGTGGAAAGGACGA
516 AACACC 3' and reverse 5'
517 GTCTCGTGGGCTCGGAGATGTGTATAAGAGACAGCCAATTCCCACTCCTTTCAAGACCT 3'
518 primers with PCR cycling conditions of 30s 95 ^{0}C, 30s 53 ^{0}C, 30s 72 ^{0}C for 18-24 cycles. PCR2

519 was performed using 5 µl of PCR1 as template using forward 5'
520 AATGATACGGCGACCACCGAGATCTACAC-10bp barcode-TCGTCGGCAGCGTC 3' and
521 reverse 5' CAAGCAGAAGACGGCATACGAGAT-10bp barcode-GTCTCGTGGGCTCGG 3'
522 primers with PCR cycling conditions of 30s 95 ^{0}C, 30s 54 ^{0}C, 30s 72 ^{0}C for 24 cycles. PCR2
523 amplicons were uniquely dual indexed with 10 bp Illumina-compatible barcodes for each
524 sample. The samples within each screen were pooled and submitted to the Genome
525 Technology Access Center, Washington University School of Medicine in St. Louis for next
526 generation sequencing on an Illumina NovaSeq-6000 with at least 100x coverage of 150 bp
527 paired end reads. Basecalls and demultiplexing were performed with Illumina's bcl2fastq2
528 software. The forward reads were analyzed using MAGeCK as described previously (53).
529 Briefly, read counts for the sgRNAs sequences were normalized and counted using the count
530 function followed by comparison between the T5 population and uninfected control using the
531 test function. The data was analyzed in R using the MAGeCKFlute package (54). Log_2Fold
532 change of sgRNAs in T5 population relative to uninfected control was plotted against -Log_{10}FDR
533 (False Discovery Rate).

534 **RNA Sequencing**

535 Cells were seeded in a 6-well plate overnight and then treated ± IFN-γ (100 U/ml) for 24 h. The
536 cells were lysed, and total RNA was extracted using QIAGEN RNeasy Mini Kit as per
537 manufacturer's instructions. The RNA samples were prepared from 3 independent biological
538 replicates and submitted to the Genome Technology Access Center, Washington University
539 School of Medicine in St. Louis, for next-generation mRNA sequencing. Library preparation was
540 performed using ~ 1ug of total RNA processed using RiboErase kits to remove ribosomal RNA
541 (Kapa Biosystems). mRNA was then fragmented in reverse transcriptase buffer and heating to
542 94 ^{0}C for 8 min. mRNA was reverse transcribed to yield cDNA using SuperScript III RT enzyme
543 (Life Technologies, per manufacturer's instructions) using random hexamers. A second strand
544 reaction was performed to yield ds-cDNA that was blunt ended, extended by adding an A base
545 to the 3' ends, and followed by ligation of Illumina sequencing adapters. Ligated fragments were
546 then amplified for 12-15 cycles using primers incorporating unique dual index tags. Fragments
547 were sequenced on an Illumina NovaSeq-6000 to generate paired end reads extending 150
548 bases. Basecalls and demultiplexing were performed with Illumina's bcl2fastq2 software. A total
549 of 1,046,709,676 reads from 18 samples were generated and the fastq files were imported into
550 CLC Genomics Workbench version 21.0.5 (QIAGEN Bioinformatics, Inc.). The reads were
551 aligned to Homo sapiens hg38 reference genome (downloaded from Ensembl via the CLC
552 Genomics Workbench) that covered 60,676 genes and 204,381 transcripts in total. The

553 expression data from the CLC Genomics Workbench were imported into R to generate heat
554 map of differentially expressed genes and compare RPKM values of ISGs across samples.

555 **CRISPR-Cas9 mediated gene deletions**

556 sgRNAs were designed using the GPP web portal and 20 bp sgRNAs were synthesized as
557 primer pairs (**Table S1.xlsx**) with overhanging BsmBI sites and ligated to BsmBI digested
558 plentiCRISPRv2. sgRNAs cloned into the plentiCRIPSRv2 plasmid was packaged into
559 lentiviruses by co-transfecting into 293T cells in equimolar ratio with pRSV-Rev, pMD2.G and
560 pMDLg/pRRE. The supernatant was collected 72 h post transfection and the virus was filtered
561 through 0.45 μm PES filter. The virus containing supernatant was titrated and was transduced
562 into different cell lines at 10% transduction efficiency for 72 h. The cells were washed and
563 incubated with puromycin (4 μg/ml for A549, 2 μg/ml for THP-1 and 1 μg/ml HFFs) for 10 days
564 to select stably transduced cells. Single cell knockouts of IRF-1, NF2, and RNF213 were
565 isolated by FACS sorting single cell per well. STAT1 KO A549 cells, ATG5 KO A549 cells and
566 RNF213 KO HFF cells were maintained at the population level. Gene deletion of host factors
567 was confirmed by western blot and Sanger sequencing of the editing site.

568 **Vacuolar size growth assay**

569 Parasite growth was monitored using a vacuolar size assay that was performed as described
570 previously (9). Briefly, host cells were seeded in 96-well μCLEAR black plates (Greiner Bio-One
571 International GmbH) for 24 h before use. For THP-1, the cells were first differentiated with 50
572 nM PMA for 48 h before addition of 100 U/ml of IFN-γ or 100 U/ml IFN-β with 10 ng/ml of TNF-α
573 for 24 h prior to infection. The cells were cultured ± 100 U/ml of IFN-γ for 24 h and then washed
574 with warm PBS. The cells were infected with parasites at MOI 0.5 for 2 h, washed with warm
575 PBS to remove extracellular parasites, and returned to culture in complete medium for different
576 intervals. Cells were fixed with 4% paraformaldehyde, permeabilized using 0.02% saponin in
577 5% FBS (Fetal bovine serum) +5% NGS (Normal goat serum) and stained to detect parasites
578 (anti-SAG1) and the parasitophorous vacuole (anti-GRA7), followed by Alexa-fluor conjugated
579 secondary antibodies, and Hoechst (100 ng/ml) to stain the nuclei. Images were acquired at a
580 magnification of 20x on a Cytation3 cell imaging multi-mode plate-based imager (BioTek). The
581 size of parasitophorous vacuole-harboring parasites (SAG1-positive GRA7 vacuoles) was
582 determined using CellProfiler 2.1.1. Data from at least 50 fields per sample in each of three
583 independent experiments were used to calculate the vacuolar size of parasites in different host
584 cells.

585 **ISRE promoter assay**

586 Cells per well were seeded at a density of 25,000 per 96-well plate and cultured overnight. The
587 cells were co-transfected with 50 ng of plasmid expressing ISRE reporter (9) and 50 ng of
588 pCMV-Red Firefly Luc Vector (Thermo Fisher Scientific # 16156) using lipofectamine LTX
589 (Thermo Fisher Scientific) according to the manufacturer's instructions. The cells were washed
590 with warm DMEM (with 10% v/v FBS) and cultured ± 100 U/ml human IFN-β for another 24 h.
591 Gaussia luciferase activity was measured in the supernatant using the Pierce Gaussia
592 luciferase glow assay kit (Thermo Fisher Scientific # 16160). Firefly luciferase activity was
593 measured in the cell lysates after removing the supernatant and washing the cells with warm
594 PBS using the Pierce Firefly luciferase glow assay kit (Thermo Fisher Scientific # 16176).
595 Luminescence was measured in Cytation3 multi-mode plate reader. ISRE promoter activity was
596 calculated by normalizing gaussian luminescence to firefly luminescence for each sample.

597 **Immunofluorescence staining**

598 Cells were seeded onto 12 mm coverslips in a 24-well overnight and then treated ± 100 U/ml
599 human IFN-γ for 24 h. The cells were washed with warm PBS and infected with CTG-GFP
600 parasites at MOI 3 for 6h. The cells were washed to remove extracellular parasites and fixed
601 with 4% paraformaldehyde for 20 min at room temperature. Cells were permeabilized and
602 blocked in using 5% FBS and 5% normal goat serum with 0.02% saponin in PBS for 30 min.
603 Cell were stained with FK2 (1:2,000; anti-mono- and poly-ubiquitinated proteins) and anti-
604 RNF213 (1:2,000) and/or anti-LC3 (1:2,000) in 1% FBS with 0.02% saponin in PBS for 90 min.
605 Cells were washed three times with PBS and incubated with Alexa-fluor conjugated secondary
606 antibodies (1:4,000) and Hoechst stain (100 ng/ml) to stain nuclei (Life Technologies) for 30
607 min. Cells were then washed three times with PBS followed by mounting in ProLong gold
608 antifade mountant (Thermo Fisher Scientific). Images were acquired using a 63x oil Plan-
609 Apochromat lens (N.A. 1.4) on an Axioskop2 MOT Plus Wide Field Fluorescence Microscope
610 (Carl Zeiss) or using a LSM880 confocal laser scanning microscope (Carl Zeiss) in the
611 Microbiology Imaging Facility, Washington University in St. Louis.

612 **Western blotting**

613 Cells were lysed using CellLytic M (Sigma) with complete mini protease inhibitor cocktail
614 (Roche). The lysates were centrifuged at 6,000 *g* for 10 min at room temperature to pellet
615 nuclear debris. Total protein was measured using BCA (bicinchoninic acid) protein assay kit
616 (Thermo Fisher Scientific). Samples were boiled at 95 ^{0}C for 15 min in Laemmli buffer
617 containing 100 mM dithiothreitol (DTT), separated by SDS-PAGE and transferred onto
618 nitrocellulose membranes. Membranes were blocked in a 1:1 mixture of Odyssey blocking

619 buffer (OBB; Li-Cor Biosciences) and PBS overnight at 4°C. Membranes were incubated with
620 primary antibodies (1:4,000) for 2 h at room temperature in a 1:1 mixture of Odyssey blocking
621 buffer and PBS with 0.1% Tween 20 (PBST). Blots were washed thrice with PBST and
622 incubated with anti-mouse IgG IR800 and anti-mouse IgG IR700 at 1:15,000 for 2 h at RT in a
623 1:1 mixture of Odyssey blocking buffer and PBST. The blot was washed thrice with PBST
624 followed by infrared imaging on a Li-Cor Odyssey imaging system.

625 ***M. tuberculosis* strains and infections**

626 *M. tuberculosis* (Mtb) was grown at 37 °C to log phase in Middlebrook 7H9 broth (BD
627 Biosciences) supplemented with 0.05% Tyloxapol, BD BBL Middlebrook OADC Enrichment (BD
628 Biosciences), and 0.2% (v/v) glycerol. H37Rv (the wild type strain) and H37Rv-GFP (GFP-
629 expressing fluorescent strain) were originally provided by William Jacobs Jr. (Albert Einstein
630 College of Medicine). H37Rv-GFP was maintained in broth containing 25 µg/mL kanamycin. For
631 *in vitro* infection assays, a log phase culture of *M. tuberculosis* was used to prepare single-cell
632 suspensions using the slow centrifugation method. Bacteria were pelleted, resuspended in cell
633 culture medium, and centrifuged at 800 rpm for 8 minutes. The supernatant was collected, and
634 the number of bacilli was estimated by measuring absorbance at 600 nm. This step was
635 repeated until a constant absorbance value was obtained. For *in vitro* infection, cells were
636 seeded in 96 well plates overnight followed by culture ± human IFN-γ (100 units/mL) for 24 h.
637 Cells were washed and infected with Mtb at MOI 0.5. After 4 hours, cells were washed three
638 times with warm DMEM to remove extracellular bacteria, and then resuspended in culture
639 medium. To estimate intracellular bacterial growth, infected cells were lysed in 0.06% SDS
640 solution at the indicated time points, and serial dilutions of the lysates were plated on 7H11 agar
641 plates (BD Biosciences, catalog no. 283810) containing BD BBL Middlebrook OADC
642 Enrichment (BD Biosciences, catalog no. 212351) and glycerol. Colony forming units (CFU)
643 were calculated 14-21 days later. For immunofluorescence assays, H37Rv-GFP infected cells
644 were fixed at 8 hpi with 4% paraformaldehyde for one hour, permeabilized and blocked in PBS
645 with 0.05% Triton X-100 and 3% BSA and stained with FK2 (1:2,000) and anti-RNF213
646 (1:2,000) overnight at 4 ^{0}C. Staining with Alexa fluorophore-conjugated secondary antibody
647 (Molecular Probes) was done for 2 h at room temperature. Following this, the samples were
648 washed with 0.1% Tween 20/PBS and mounted using Prolong Gold antifade (Thermo Fisher
649 Scientific, # P36930). Images were captured using a Nikon Eclipse Ti confocal microscope
650 (Nikon Instruments Inc.) equipped with a 60X apochromat oil-objective lens and analyzed using
651 NIS-Elements version 4.40 (Nikon).

652 **Vesicular Stomatitis virus (VSV) culture and infections**

653 Recombinant vesicular stomatitis virus (VSV) expressing enhanced green fluorescent protein
654 (eGFP; VSV-GFP) (55) was propagated as previously described (56) in either African Green
655 Monkey kidney Vero E6 (CRL-1586, ATCC) or MA104 cells (CRL-2378.1). Vero E6 cells and
656 MA104 cells were cultured in complete DMEM media and complete M199 media, respectively.
657 Viral titers were determined by standard plaque assays. Cells were seeded at 10,000 per well in
658 24-well plates and cultured overnight followed by culture in ± 100 U/ml human IFN-β for 24 h.
659 The cells were washed and infected with VSV-GFP at MOI 1 for 24 h, as described previously
660 (57). GFP intensity was determined by scanning with an Amersham Typhoon 5 (GE) and
661 images quantified by ImageJ. The number of total intensities subtracted from background was
662 computed for each treatment and $\log_{10}$ transformed.

663 **Immuno-electron microscopy**

664 Wild type A549 cells were pre-activated with IFN-γ (100 U/ml) 24 h prior to infection with CTG
665 for 6h. The cells were trypsinized and fixed in 4% paraformaldehyde/0.01% glutaraldehyde
666 (Polysciences Inc., Warrington, PA) in 100 mM PIPES/0.5 mM $MgCl_2$, pH 7.2 for 1 h at 4
667 °C. Samples were then embedded in 10% gelatin and infiltrated overnight with 2.3 M
668 sucrose/20% polyvinyl pyrrolidone in PIPES/$MgCl_2$ at 4 °C. Samples were trimmed, frozen in
669 liquid nitrogen, and sectioned with a Leica Ultracut UCT7 cryo-ultramicrotome (Leica
670 Microsystems Inc., Bannockburn, IL). Ultrathin sections of 50 nm were blocked with 5% FBS
671 (fetal bovine serum)/5% NGS (normal goat serum) for 30 min and subsequently incubated with
672 rabbit anti-RNF213 antibody for 1 h at room temperature. Following washes in block buffer,
673 sections were incubated with secondary anti-rabbit IgG antibody conjugated to 18 nm colloidal
674 gold (Jackson ImmunoResearch Laboratories, Inc., West Grove, PA) for 1 h. Sections were
675 stained with 0.3% uranyl acetate/2% methyl cellulose and viewed by transmission electron
676 microscopy. All labeling experiments were conducted in parallel with controls omitting the
677 primary antibody.

678 **Transmission electron microscopy**

679 Wild type A549 cells were pre-activated with IFN-γ (100 U/ml) 24 h prior to infection with CTG
680 for 6h. The cells were trypsinized and fixed freshly prepared mixture of 1% glutaraldehyde
681 (Polysciences Inc, Warrington, PA) and 1% osmium tetroxide (Polysciences Inc.) in 50 mM
682 phosphate buffer at 4ºC for 30 min. Samples were then rinsed extensively in cold dH_20 prior to
683 en bloc staining with 1% aqueous uranyl acetate (Ted Pella Inc., Redding, CA) at 4 ºC for 3
684 h. Following several rinses in dH_20, samples were dehydrated in a graded series of ethanol and

685 embedded in Eponate 12 resin (Ted Pella Inc.). Sections of 95 nm were cut with a Leica
686 Ultracut UCT ultramicrotome (Leica Microsystems Inc., Bannockburn, IL), stained with uranyl
687 acetate and lead citrate, and viewed on a JEOL 1200 EX transmission electron microscope
688 (JEOL USA Inc., Peabody, MA) equipped with an AMT 8 megapixel digital camera and AMT
689 Image Capture Engine V602 software (Advanced Microscopy Techniques, Woburn, MA).

690 **Statistical analysis**

691 All experiments were performed in 3 independent biological repeats unless mentioned
692 otherwise. Statistical analysis for each experiment was performed on the combined data in
693 PRISM. Significance values and tests performed are included in the figure legends.

694

695 ## References

696 1. Sibley LD. 2011. Invasion and intracellular survival by protozoan parasites.
697 Immunological Reviews 240:72-91.
698 2. Blader IJ, Coleman BI, Chen CT, Gubbels MJ. 2015. Lytic Cycle of Toxoplasma gondii: 15
699 Years Later. Annu Rev Microbiol 69:463-85.
700 3. Clough B, Frickel EM. 2017. The Toxoplasma Parasitophorous Vacuole: An Evolving Host-
701 Parasite Frontier. Trends Parasitol 33:473-488.
702 4. Khan IA, Moretto M. 2022. Immune responses to Toxoplasma gondii. Curr Opin
703 Immunol 77:102226.
704 5. Frickel EM, Hunter CA. 2021. Lessons from Toxoplasma: Host responses that mediate
705 parasite control and the microbial effectors that subvert them. J Exp Med 218.
706 6. Yap GS, Sher A. 1999. Effector cells of both nonhemopoietic and hemopoietic origin are
707 required for interferon (IFN)-gamma- and tumor necrosis factor (TNF)-alpha- dependent
708 host resistance to the intracellular pathogen, *Toxoplasma gondii*. J Exp Med 189:1083-
709 1091.
710 7. Suzuki Y, Orellana MA, Schreiber RD, Remington JS. 1988. Interferon-g: the major
711 mediator of resistance against *Toxoplasma gondii*. Science 240:516-518.
712 8. Han SJ, Melichar HJ, Coombes JL, Chan SW, Koshy AA, Boothroyd JC, Barton GM, Robey
713 EA. 2014. Internalization and TLR-dependent type I interferon production by monocytes
714 in response to Toxoplasma gondii. Immunol Cell Biol 92:872-81.
715 9. Matta SK, Olias P, Huang Z, Wang Q, Park E, Yokoyama WM, Sibley LD. 2019.
716 *Toxoplasma gondii* effector TgIST blocks type I interferon signaling to promote infection.
717 Proc Natl Acad Sci U S A 116:17480-17491.
718 10. Mostafavi S, Yoshida H, Moodley D, LeBoite H, Rothamel K, Raj T, Ye CJ, Chevrier N,
719 Zhang SY, Feng T, Lee M, Casanova JL, Clark JD, Hegen M, Telliez JB, Hacohen N, De Jager
720 PL, Regev A, Mathis D, Benoist C, Immunological Genome Project C. 2016. Parsing the
721 Interferon Transcriptional Network and Its Disease Associations. Cell 164:564-78.
722 11. Rusinova I, Forster S, Yu S, Kannan A, Masse M, Cumming H, Chapman R, Hertzog PJ.
723 2013. Interferome v2.0: an updated database of annotated interferon-regulated genes.
724 Nucleic Acids Res 41:D1040-6.

725 12. Howard JC, Hunn JP, Steinfeldt T. 2011. The IRG protein-based resistance mechanism in
726 mice and its relation to virulence in *Toxoplasma gondii*. Curr Opin Microbiol 14:414-21.
727 13. Gazzinelli RT, Mendonca-Neto R, Lilue J, Howard J, Sher A. 2014. Innate resistance
728 against Toxoplasma gondii: an evolutionary tale of mice, cats, and men. Cell Host
729 Microbe 15:132-8.
730 14. MacMicking JD. 2012. Interferon-inducible effector mechanisms in cell-autonomous
731 immunity. Nat Rev Immunol 12:367-82.
732 15. Zhao Z, Fux B, Goodwin M, Dunay IR, Strong D, Miller BC, Cadwell K, Delgado MA,
733 Ponpuak M, Green KG, Schmidt RE, Mizushima N, Deretic V, Sibley LD, Virgin HW. 2008.
734 Autophagosome-independent essential function for the autophagy protein Atg5 in
735 cellular immunity to intracellular pathogens. Cell Host Microbe 4:458-469.
736 16. Ohshima J, Lee Y, Sasai M, Saitoh T, Su Ma J, Kamiyama N, Matsuura Y, Pann-Ghill S,
737 Hayashi M, Ebisu S, Takeda K, Akira S, Yamamoto M. 2014. Role of mouse and human
738 autophagy proteins in IFN-gamma-induced cell-autonomous responses against
739 *Toxoplasma gondii*. J Immunol 192:3328-35.
740 17. Choi J, Park S, Biering S, Selleck EM, Liu C, Zhang X, Fujita N, Saitoh T, Akira S, Yoshimori
741 T, Sibley LD, Hwang S, Virgin HW. 2014. The parasitophorous vacuole membrane of
742 *Toxoplasma gondii* is targeted for disruption by ubiquitin-like conugation systems of
743 autophagy. Immunity in press.
744 18. Hoffmann C, Ernst M, Meyer P, Wolf E, Rosenkranz T, Plettenberg A, Stoehr A, Horst HA,
745 Marienfeld K, Lange C. 2007. Evolving characteristics of toxoplasmosis in patients
746 infected with human immunodeficiency virus-1: clinical course and Toxoplasma gondii-
747 specific immune responses. Clin Microbiol Infect 13:510-5.
748 19. Meira CS, Pereira-Chioccola VL, Vidal JE, de Mattos CC, Motoie G, Costa-Silva TA, Gava R,
749 Frederico FB, de Mattos LC, Toxoplasma G. 2014. Cerebral and ocular toxoplasmosis
750 related with IFN-gamma, TNF-alpha, and IL-10 levels. Front Microbiol 5:492.
751 20. Murray HW, Granger AM, Teitelbaum RF. 1991. Gamma interferon-activated human
752 macrophages and *Toxoplasma gondii*, *Chalmydia psittaci*, and *Leishmania donovani*:
753 antimicrobial role of limiting intracellular iron. Infection and Immunity 59:4684-4686.
754 21. Nathan CF, Murray HW, Weibe ME, Rubin BY. 1983. Indentification of interferon gamma
755 as the lymphokine that activates human macrophage oxidative metabolism and
756 antimicrobial activity. J Exp Med 158:670-689.
757 22. Orellana MA, Suzuki Y, Araujo F, Remington JS. 1991. Role of beta interferon in
758 resistance to Toxoplasma gondii infection. Infect Immun 59:3287-90.
759 23. Schmitz JL, Carlin JM, Borden EC, Byrne GI. 1989. Beta interferon inhibits Toxoplasma
760 gondii growth in human monocyte-derived macrophages. Infect Immun 57:3254-6.
761 24. Matta SK, Rinkenberger N, Dunay IR, Sibley LD. 2021. Toxoplasma gondii infection and
762 its implications within the central nervous system. Nat Rev Microbiol 19:467-480.
763 25. Pfefferkorn ER. 1984. Interferon-gamma blocks the growth of *Toxoplasma gondii* in
764 human fibroblasts by inducing the host to degrade tryptophan. Proc Natl Acad Sci (USA)
765 81:908-912.
766 26. Daubener W, Spors B, Hucke C, Adam R, Stins M, Kim KS, Schroten H. 2001. Restriction
767 of Toxoplasma gondii growth in human brain microvascular endothelial cells by
768 activation of indoleamine 2,3-dioxygenase. Infect Immun 69:6527-31.

769 27. Selleck EM, Orchard RC, Lassen KG, Beatty WL, Xavier RJ, Levine B, Virgin HW, Sibley LD.
770 2015. A noncanonical autophagy pathway restricts *Toxoplasma gondii* growth in a
771 strain-specific manner in IFN-gamma-activated human cells. MBio 6:e01157-15.
772 28. Bhushan J, Radke JB, Perng YC, McAllaster M, Lenschow DJ, Virgin HW, Sibley LD. 2020.
773 ISG15 Connects Autophagy and IFN-gamma-Dependent Control of Toxoplasma gondii
774 Infection in Human Cells. mBio 11.
775 29. Clough B, Wright JD, Pereira PM, Hirst EM, Johnston AC, Henriques R, Frickel EM. 2016.
776 K63-Linked Ubiquitination Targets Toxoplasma gondii for Endo-lysosomal Destruction in
777 IFNgamma-Stimulated Human Cells. PLoS Pathog 12:e1006027.
778 30. Hernandez D, Walsh S, Saavedra Sanchez L, Dickinson MS, Coers J. 2022. Interferon-
779 Inducible E3 Ligase RNF213 Facilitates Host-Protective Linear and K63-Linked
780 Ubiquitylation of Toxoplasma gondii Parasitophorous Vacuoles. mBio
781 doi:10.1128/mbio.01888-22:e0188822.
782 31. Johnston AC, Piro A, Clough B, Siew M, Virreira Winter S, Coers J, Frickel EM. 2016.
783 Human GBP1 does not localize to pathogen vacuoles but restricts Toxoplasma gondii.
784 Cell Microbiol 18:1056-64.
785 32. Fisch D, Bando H, Clough B, Hornung V, Yamamoto M, Shenoy AR, Frickel EM. 2019.
786 Human GBP1 is a microbe-specific gatekeeper of macrophage apoptosis and pyroptosis.
787 EMBO J 38:e100926.
788 33. Fisch D, Clough B, Khan R, Healy L, Frickel EM. 2022. Toxoplasma-proximal and distal
789 control by GBPs in human macrophages. Pathog Dis 79.
790 34. Rinkenberger N, Abrams ME, Matta SK, Schoggins JW, Alto NM, Sibley LD. 2021.
791 Overexpression screen of interferon-stimulated genes identifies RARRES3 as a restrictor
792 of Toxoplasma gondii infection. Elife 10.
793 35. Fentress SJ, Behnke MS, Dunay IR, Mashayekhi M, Rommereim LM, Fox BA, Bzik DJ,
794 Taylor GA, Turk BE, Lichti CF, Townsend RR, Qiu W, Hui R, Beatty WL, Sibley LD. 2010.
795 Phosphorylation of immunity-related GTPases by a Toxoplasma gondii-secreted kinase
796 promotes macrophage survival and virulence. Cell Host Microbe 8:484-95.
797 36. Doench JG, Fusi N, Sullender M, Hegde M, Vaimberg EW, Donovan KF, Smith I, Tothova
798 Z, Wilen C, Orchard R, Virgin HW, Listgarten J, Root DE. 2016. Optimized sgRNA design to
799 maximize activity and minimize off-target effects of CRISPR-Cas9. Nat Biotechnol
800 34:184-191.
801 37. Li W, You L, Cooper J, Schiavon G, Pepe-Caprio A, Zhou L, Ishii R, Giovannini M,
802 Hanemann CO, Long SB, Erdjument-Bromage H, Zhou P, Tempst P, Giancotti FG. 2010.
803 Merlin/NF2 suppresses tumorigenesis by inhibiting the E3 ubiquitin ligase CRL4(DCAF1)
804 in the nucleus. Cell 140:477-90.
805 38. Doench JG. 2018. Am I ready for CRISPR? A user's guide to genetic screens. Nat Rev
806 Genet 19:67-80.
807 39. Feng H, Zhang YB, Gui JF, Lemon SM, Yamane D. 2021. Interferon regulatory factor 1
808 (IRF1) and anti-pathogen innate immune responses. PLoS Pathog 17:e1009220.
809 40. James MF, Han S, Polizzano C, Plotkin SR, Manning BD, Stemmer-Rachamimov AO,
810 Gusella JF, Ramesh V. 2009. NF2/merlin is a novel negative regulator of mTOR complex
811 1, and activation of mTORC1 is associated with meningioma and schwannoma growth.
812 Mol Cell Biol 29:4250-61.

813 41. White SM, Avantaggiati ML, Nemazanyy I, Di Poto C, Yang Y, Pende M, Gibney GT,
814 Ressom HW, Field J, Atkins MB, Yi C. 2019. YAP/TAZ Inhibition Induces Metabolic and
815 Signaling Rewiring Resulting in Targetable Vulnerabilities in NF2-Deficient Tumor Cells.
816 Dev Cell 49:425-443 e9.
817 42. Otten EG, Werner E, Crespillo-Casado A, Boyle KB, Dharamdasani V, Pathe C, Santhanam
818 B, Randow F. 2021. Ubiquitylation of lipopolysaccharide by RNF213 during bacterial
819 infection. Nature 594:111-116.
820 43. Houzelstein D, Simon-Chazottes D, Batista L, Tokuda S, Langa Vives F, Flamand M,
821 Montagutelli X, Panthier JJ. 2021. The ring finger protein 213 gene (Rnf213) contributes
822 to Rift Valley fever resistance in mice. Mamm Genome 32:30-37.
823 44. Taniguchi T, Ogasawara K, Takaoka A, Tanaka N. 2001. IRF family of transcription factors
824 as regulators of host defense. Annu Rev Immunol 19:623-55.
825 45. O'Connell BC, Harper JW. 2007. Ubiquitin proteasome system (UPS): what can
826 chromatin do for you? Curr Opin Cell Biol 19:206-14.
827 46. Thery F, Martina L, Asselman C, Zhang Y, Vessely M, Repo H, Sedeyn K, Moschonas GD,
828 Bredow C, Teo QW, Zhang J, Leandro K, Eggermont D, De Sutter D, Boucher K,
829 Hochepied T, Festjens N, Callewaert N, Saelens X, Dermaut B, Knobeloch KP, Beling A,
830 Sanyal S, Radoshevich L, Eyckerman S, Impens F. 2021. Ring finger protein 213
831 assembles into a sensor for ISGylated proteins with antimicrobial activity. Nat Commun
832 12:5772.
833 47. Walsh SC, Reitano JR, Dickinson MS, Kutsch M, Hernandez D, Barnes AB, Schott BH,
834 Wang L, Ko DC, Kim SY, Valdivia RH, Bastidas RJ, Coers J. 2022. The bacterial effector
835 GarD shields Chlamydia trachomatis inclusions from RNF213-mediated ubiquitylation
836 and destruction. Cell Host Microbe doi:10.1016/j.chom.2022.08.008.
837 48. Ahel J, Lehner A, Vogel A, Schleiffer A, Meinhart A, Haselbach D, Clausen T. 2020.
838 Moyamoya disease factor RNF213 is a giant E3 ligase with a dynein-like core and a
839 distinct ubiquitin-transfer mechanism. Elife 9.
840 49. Burg JL, Perlman D, Kasper LH, Ware PL, Boothroyd JC. 1988. Molecular analysis of the
841 gene encoding the major surface antigen of *Toxoplasma gondii*. J Immunol 141:3584-
842 3591.
843 50. Alaganan A, Fentress SJ, Tang K, Wang Q, Sibley LD. 2013. Toxoplasma GRA7 effector
844 increases turnover of immunity-related GTPases and contributes to acute virulence in
845 the mouse. Proc Natl Acad Sci (USA) 111:1126-1131.
846 51. Sanjana NE, Shalem O, Zhang F. 2014. Improved vectors and genome-wide libraries for
847 CRISPR screening. Nat Methods 11:783-784.
848 52. Gibson DG. 2011. Enzymatic assembly of overlapping DNA fragments. Methods Enzymol
849 498:349-61.
850 53. Li W, Xu H, Xiao T, Cong L, Love MI, Zhang F, Irizarry RA, Liu JS, Brown M, Liu XS. 2014.
851 MAGeCK enables robust identification of essential genes from genome-scale
852 CRISPR/Cas9 knockout screens. Genome Biol 15:554.
853 54. Wang B, Wang M, Zhang W, Xiao T, Chen CH, Wu A, Wu F, Traugh N, Wang X, Li Z, Mei S,
854 Cui Y, Shi S, Lipp JJ, Hinterndorfer M, Zuber J, Brown M, Li W, Liu XS. 2019. Integrative
855 analysis of pooled CRISPR genetic screens using MAGeCKFlute. Nat Protoc 14:756-780.

856 55. Cherry S, Doukas T, Armknecht S, Whelan S, Wang H, Sarnow P, Perrimon N. 2005.
857 Genome-wide RNAi screen reveals a specific sensitivity of IRES-containing RNA viruses to
858 host translation inhibition. Genes Dev 19:445-52.
859 56. Li B, Ding S, Feng N, Mooney N, Ooi YS, Ren L, Diep J, Kelly MR, Yasukawa LL, Patton JT,
860 Yamazaki H, Shirao T, Jackson PK, Greenberg HB. 2017. Drebrin restricts rotavirus entry
861 by inhibiting dynamin-mediated endocytosis. Proc Natl Acad Sci U S A 114:E3642-E3651.
862 57. Ding S, Zhu S, Ren L, Feng N, Song Y, Ge X, Li B, Flavell RA, Greenberg HB. 2018.
863 Rotavirus VP3 targets MAVS for degradation to inhibit type III interferon expression in
864 intestinal epithelial cells. Elife 7.
865
866

867 **Figures Legends**

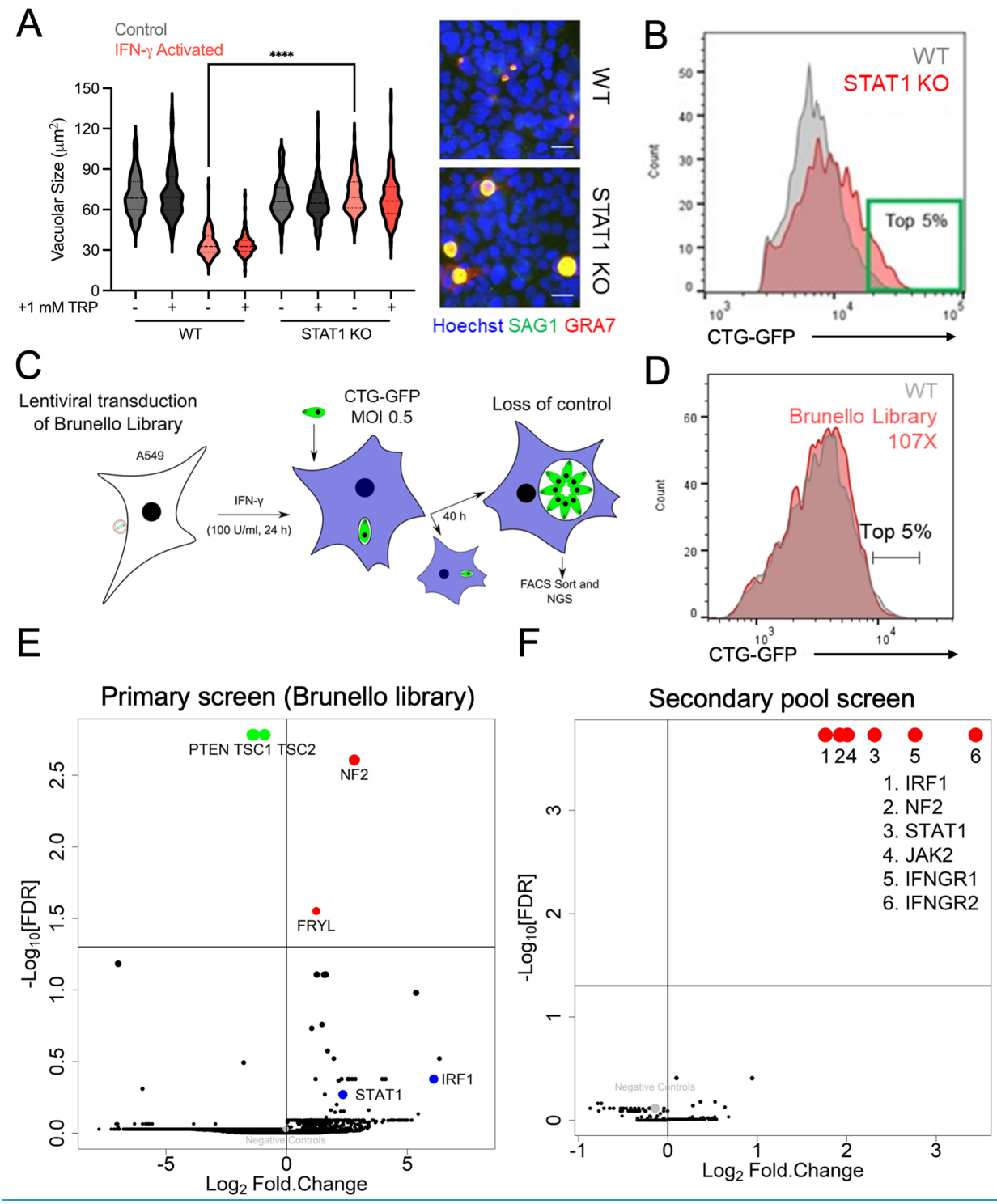

868

869 **Figure 1** Design and implementation of genome-wide CRISPR screens for loss of IFN-γ-
870 mediated parasite growth restriction in human cells (A) Tryptophan (TRP)-independent
871 restriction of *T. gondii* in lung alveolar epithelial A549 cells. Wild type (WT) and STAT1 knock

872 out (KO) A549 cells (**Fig. S1A**) were treated ± IFN-γ (100 Units/ml) 24 h prior to infection with
873 type III CTG strain of *T. gondii.* The cells were either left untreated (Control) or supplemented
874 with 1 mM TRP for 40 h. Growth was measured by vacuolar size (microns^2) for at least 3
875 biological replicates with ≥ 30 images per sample and replicate. Violin plot shows mean
876 vacuolar size per image with black bar representing the median. **** $P < 0.0001$ using unpaired
877 Two-tailed t-test with Welch's correction. Representative images of WT and STAT1 KO A549
878 cells (+IFN-γ +TRP) infected with CTG and analyzed at 40 h hpi. Nuclei labeled with Hoechst
879 (blue), parasites with anti-SAG1 (green) and the vacuole membrane with anti-GRA7 (red). Scale
880 bar = 20 microns. (B) IFN-γ activated WT vs. STAT1 KO A549 cells infected with CTG
881 expressing GFP (CTG-GFP) were fixed 40 hpi and analyzed by flow cytometry. Histogram
882 shows GFP positive (CTG-GFP infected) cells. Green box defines the top 5% of CTG-GFP
883 expressing cells. (C) Design of genome-wide CRISPR-Cas9 to identify factors involved in IFN-γ
884 mediated parasite growth restriction in human (A549) cells. (D) The Brunello library (36) was
885 transduced into A549 cells at ~100X coverage. Histogram of CTG-GFP infection analyzed at 40
886 hpi in IFN-γ activated control (WT) and Brunello library transduced A549 cells. (E) Primary
887 genome-wide CRISPR screen showing Log_2 fold change in sgRNAs from the top 5% of CTG-
888 GFP expressing cells (T5) compared to uninfected cells plotted against $-log_{10}$ false discovery
889 rate (FDR) for all 4 independent replicates combined. Genes for significantly enriched sgRNAs
890 (red) vs. significantly depleted sgRNAs in the T5 pool (green) are labeled. (F) Secondary
891 CRISPR screen consisting of a sub-pool of 224 genes that were significantly enriched in the T5
892 population (Log_2Fold Change > 1 and $P < 0.05$) in at least 2 out of the 4 replicates of the
893 primary Brunello screen (**Fig. S1B**). Log_2 Fold Change is plotted against $-log_{10}$ FDR for all 4
894 independent replicates combined.
895
896

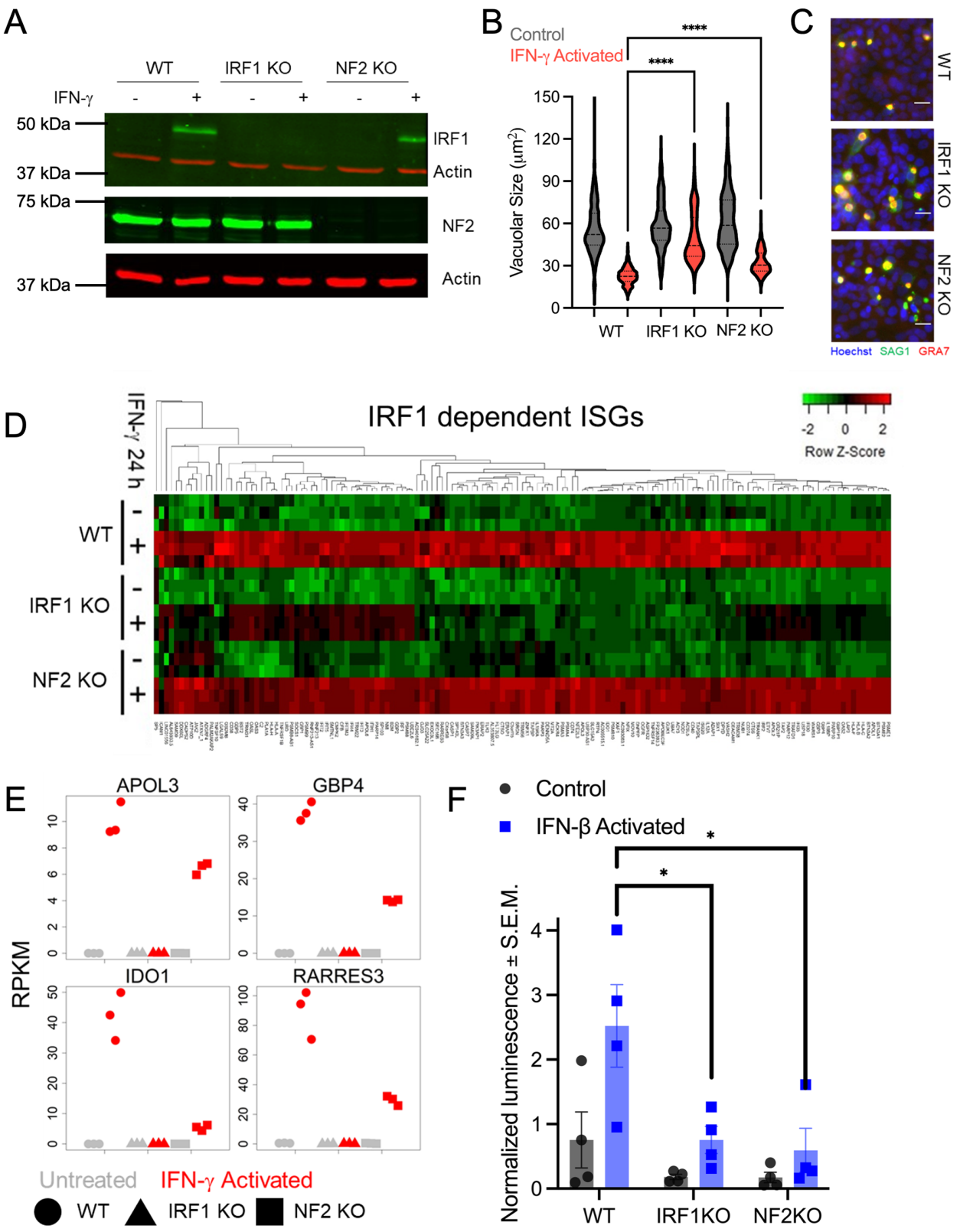

Figure 2 NF2 dampens IFN-γ-mediated growth restriction by inhibiting ISG induction. (A) Immunoblots for IRF-1 and NF2 in wild type, IRF1 KO, and NF2 KO A549 cells (**Fig. S2A and**

900 **S2B**). Actin was used as a loading control. (B) Wild type, IRF1 KO, and NF2 KO A549 cells
901 treated ± IFN-g (100 U/ml) for 24 h, infected with CTG strain *T. gondii*, and evaluated for growth
902 restriction at 40 hpi. Violin plots show mean vacuolar size per image with the black bar
903 representing the median for at least 3 biological replicates containing at least 30 images per
904 sample and replicate. **** $P < 0.0001$ using Ordinary one-way ANOVA with Turkey's multiple
905 comparison test. (C) Representative images of IFN-γ activated wild type, IRF1 KO and NF2 KO
906 A549 cells infected with CTG and analyzed at 40 hpi. Cells were labelled with Hoechst for nuclei
907 (blue), anti-SAG1 for parasites (green), and anti-GRA7 for vacuoles (red). Scale bar = 20
908 microns. (D) Global transcriptional profiling from A549 cells treated ± IFN-γ (100 U/ml) for 24 h.
909 Heat maps depict genes that were induced in WT but not in IRF1 KO cells from 3 biological
910 replicates clustered using 1-Pearson 1 - Pearson distance and average linkage on normalized
911 Log_2 (RPKM) values. Normalized Z-scores are color-scaled from down-regulation (green) to
912 upregulation (red). (E) RPKM values showing partial induction of select ISGs in NF2 KO cells
913 upon IFN-γ activation compared to WT cells. (F) ISRE promoter activity from A549 cells
914 transfected with ISRE reporter plasmid expressing Gaussia luciferase (9) and control pCMV-
915 Red Firefly Luc plasmid (Thermo Fisher Scientific) for 24 h. Bar plot shows mean ± S.E.M
916 Gaussia luciferase activity normalized to firefly luciferase activity for 4 independent biological
917 replicates. * $P < 0.05$ using Two-way ANOVA with Turkey's multiple comparison test.
918

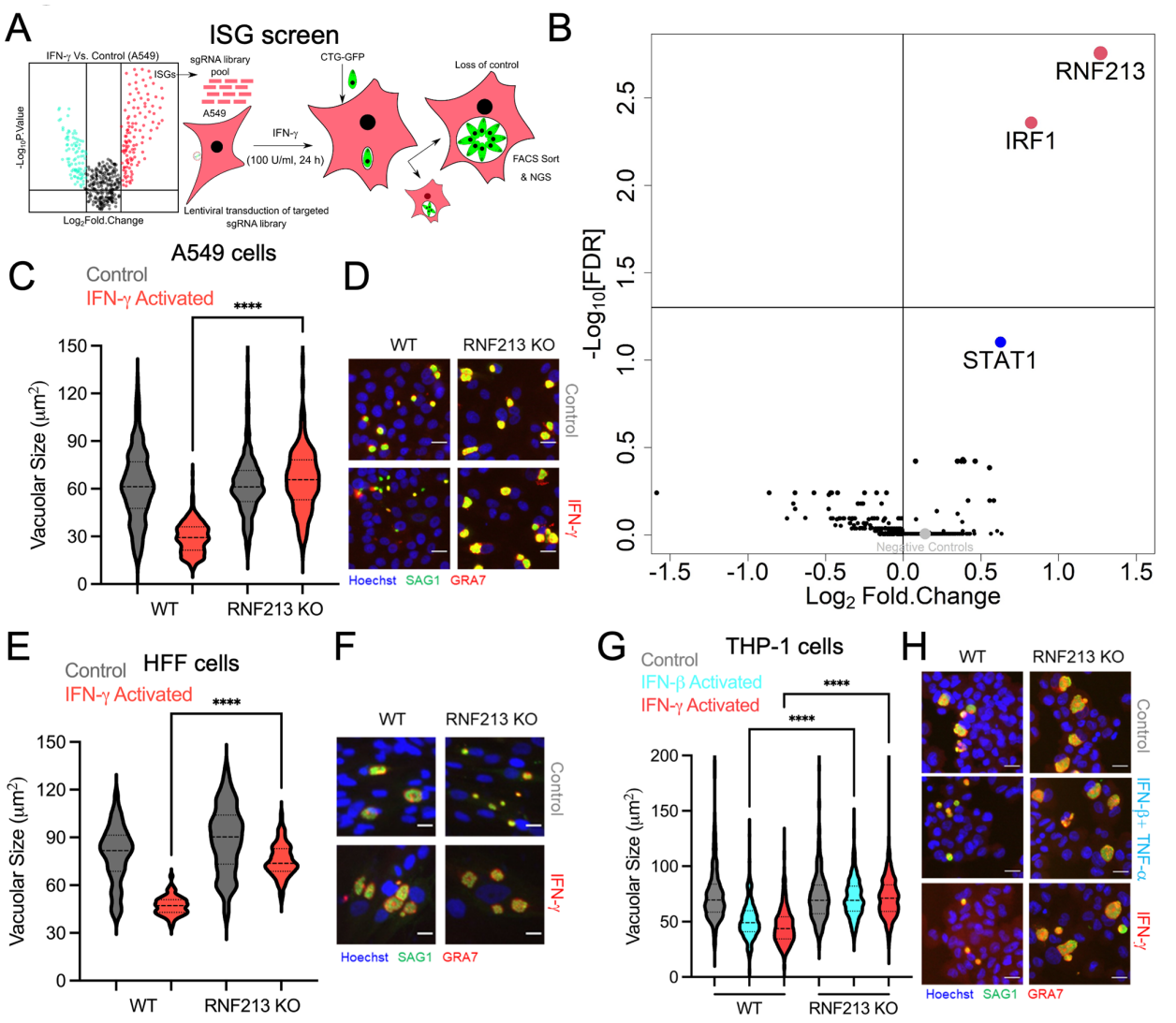

Figure 3 CRISPR-Cas9 screen identifies RNF213 as the primary ISG required for IFN-γ-mediated growth restriction of *T. gondii* in human cells (A) Design of ISG targeted sgRNA CRISPR-Cas9 screen using a sub-pool of ISGs that were previously shown to be upregulated in A549 cells treated with IFN-γ (34). (B) Targeted sgRNA screen of ISGs upregulated by IFN-γ identified two genes that were significantly depleted in the top 5% of CTG-GFP expressing cells (red). Log_2 Fold Change is plotted against -log_{10} FDR for all 4 independent replicates combined. (C) Wild type and RNF213 KO A549 cells (**Fig. S4A and 4B**) treated ± IFN-g (100 U/ml) for 24 h, infected with CTG strain *T. gondii*, and evaluated for growth restriction by quantifying vacuolar size. Vacuolar growth of parasites was measured for at least 3 independent biological replicates with 30 images per sample and replicate. Violin plot shows mean vacuolar size per image with black bar representing the median. ****$P < 0.01$ using two-tailed unpaired Student's t-test with Welch's correction. (D) Representative images showing nuclei stained with Hoechst

932 (blue), parasites stained with anit-SAG1 (green), and the vacuole membrane stained with anti-
933 GRA7 (red). Scale bar = 20 microns. (E) Vacuolar growth of parasites at 40 hpi in ± IFN-γ
934 activated WT and RNF213 KO human foreskin fibroblast (HFF) cells. Violin plot shows mean
935 vacuolar size (μm^2) per image with black bar as median for at least 3 independent biological
936 replicates with at least 30 images per sample and replicate. **** $P < 0.0001$ two-tailed unpaired
937 Student's t-test with Welch's correction. (F) Representative images of the vacuole size in control
938 and IFN-γ activated WT and RNF213 KO HFF cells infected with CTG and analyzed at 40 hpi.
939 Nuclei were labelled with Hoechst (blue), the parasite with anti-SAG1 (green) and the vacuole
940 membrane with anti-GRA7 (red) with bar = 20 μm. (G) Vacuolar growth of parasites at 40 hpi in
941 control, IFN-β+TNF-α and IFN-γ activated WT and RNF213 KO human THP-1 macrophages.
942 Violin plot shows mean vacuolar size (μm^2) per image with black bar as median for at least 3
943 biological replicates with at least 30 images per sample and replicate. **** $P < 0.0001$ using
944 Ordinary one-way ANOVA with Turkey's multiple comparisons test. (H) Representative images
945 of control, IFN-β+TNF-α and IFN-γ activated WT and RNF213 KO THP-1 cells infected with
946 CTG and analyzed at 40 hpi. Nuclei are labelled with Hoechst (blue), parasites with anti-SAG1
947 (green) and the vacuole membrane with anti-GRA7 (red). Scale bar = 20 μm.
948

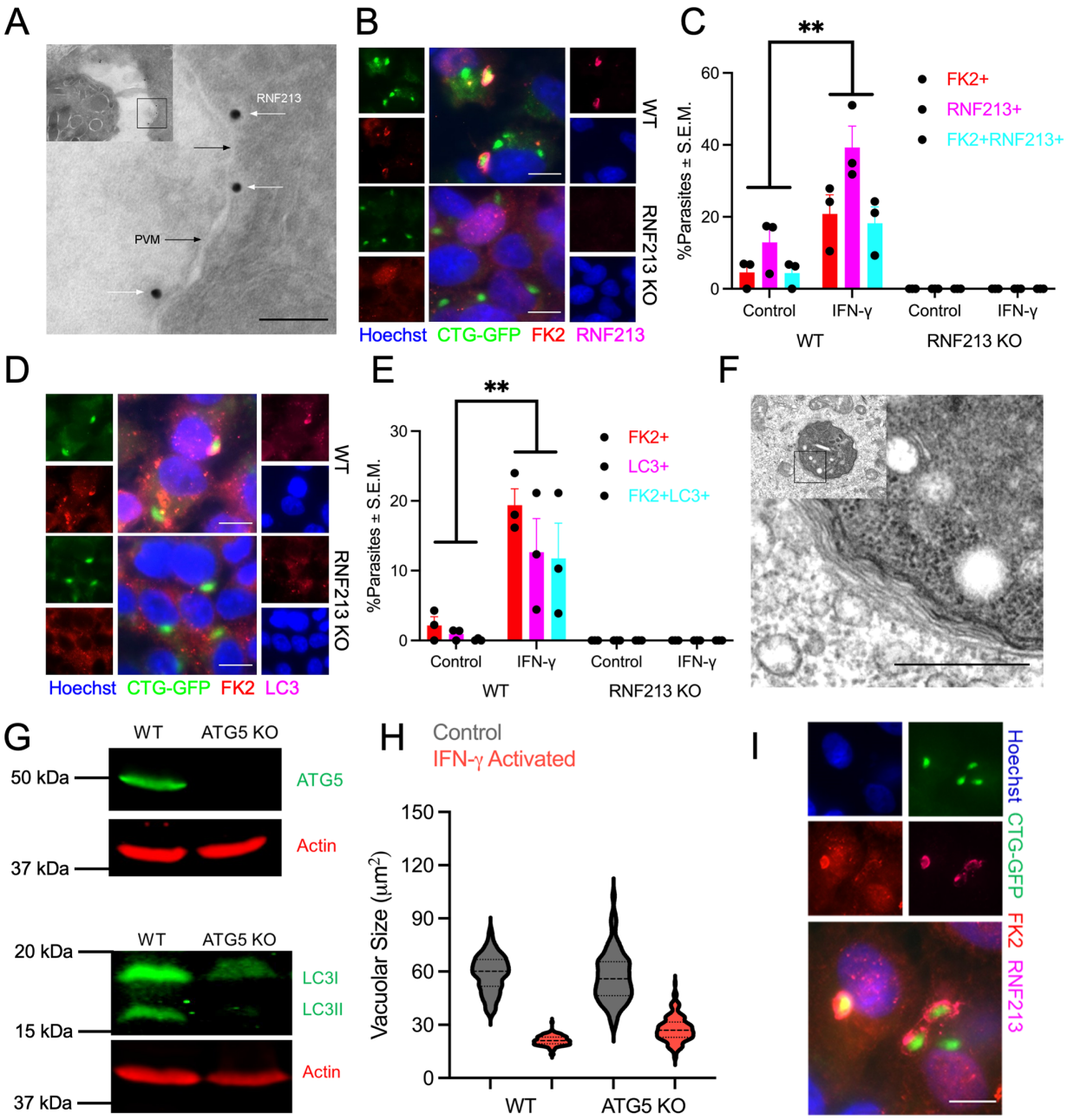

Figure 4 RNF213 co-localized with ubiquitinated parasite-containing vacuoles. (A) Immuno-EM labeling of RNF213 in IFN-γ activated wild type A549 cell infected with CTG parasite (inset) at 6 hpi. Parasite vacuolar membrane (PVM). Bar = 100 nm. (B) Representative images of WT and RNF213 KO A549 cells infected with CTG-GFP at 6 hpi. Cells were stained with FK2 (mono-poly ubiquitin; red) and anti-RNF213 (magenta). Nuclei were labelled with Hoechst (blue) and parasites were GFP labelled (green), Bar = 10 μm. (C) Quantification of FK2+ (red), RNF213+ (magenta) and FK2+RNF213+ (cyan) parasites for at least 3 biological replicates, mean ±

957 S.E.M. ** $P < 0.01$ using Two-way ANOVA with Turkey's multiple comparisons test. (D)
958 Representative images of wild type and RNF213 KO A549 cells infected with CTG-GFP at 6 hpi.
959 The cells were stained with FK2 (red) and anti-LC3B (magenta). Nuclei were labelled with
960 Hoechst (blue) and parasites were GFP labelled (green). Scale bar = 10 μm. (E) Quantification
961 of FK2+ (red), LC3+ (magenta) and FK2+LC3+ (cyan) parasites for at least 3 biological
962 replicates, mean ± S.E.M. ** $P < 0.01$ using Two-way ANOVA with Turkey's multiple
963 comparisons test. (F) Transmission electron microscopic image of IFN-γ activated wild type
964 A549 cell infected with CTG parasite (inset) at 6 hpi. Wrapping by multiple membranes is
965 highlighted in the magnified view. Bar = 500 nm. (G) ATG5 (top) and LC3B (bottom)
966 immunoblots of WT and ATG5 KO A549 cells. Actin was used as loading control. (H) Vacuolar
967 growth of CTG parasite at 40 hpi in ± IFN-γ activated wild type and ATG KO cells. Violin plot
968 shows mean vacuolar size (μm^2) per image with black bar as median for an experiment with at
969 least 30 images per sample. (I) Representative image of IFN-γ activated ATG5 KO A549 cells
970 infected with CTG-GFP at 6 hpi. The cells are stained with FK2 (red) and anti-RNF213
971 (magenta). Bar = 10 μm.
972

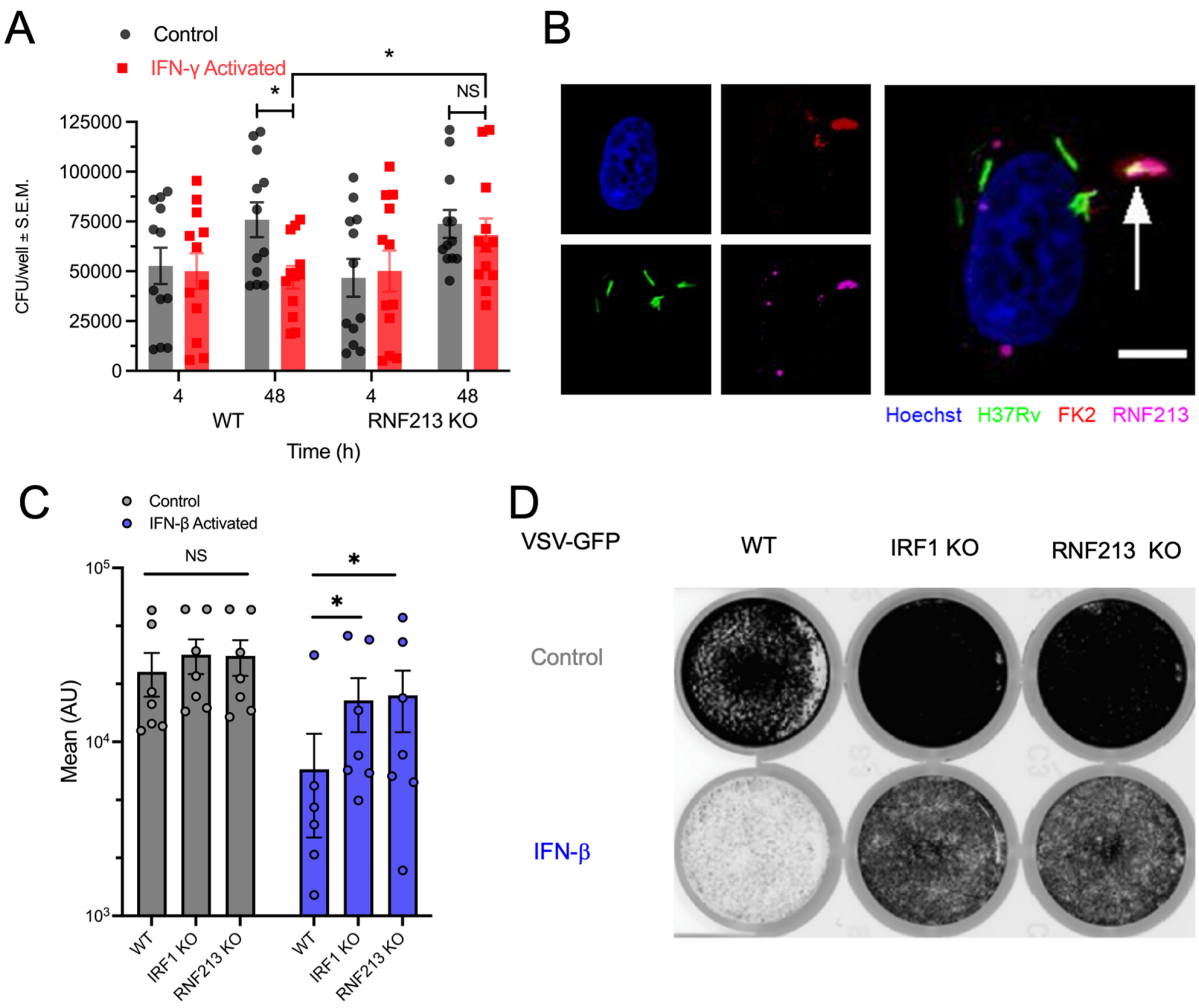

Figure 5 RNF213 is required for interferon-mediated control of intracellular bacterial and viral infection in human cells. (A) Mtb growth in ± IFN-γ (100 U/ml for 24 h) activated WT and RNF213 KO A549 cells at 4 and 48 hpi. Data shows mean colony forming units (CFU) per well ± S.E.M. from four independent experiments each with 3 internal replicates. * $P < 0.05$ using two-tailed unpaired Student's t-test. (B) Representative image showing co-localization of Mtb (green) with ubiquitin and RNF213. Cells were stained with FK2 (red) and RNF213 (magenta) in IFN-γ activated A549 cells that were analyzed at 8 hpi. Arrow depicts FK2+ and RNF213+ Mtb. Nuclei are labelled with Hoechst (blue). Scale bar = 5 μm. (C) Control and IFN-β (24 h, 100 U/ml) activated WT, IRF1 KO and RNF213 KO A549 cells infected with MOI 1 VSV-GFP (recombinant vesicular stomatitis virus expressing enhanced green fluorescent protein) at 24 hpi. Bar plot shows levels of GFP expression plotted as mean arbitrary units (AU). Data are means ± SEM for 7 independent biological replicates. * $P < 0.05$ using Two-way ANOVA with Dunnett's

986 multiple comparison test. (D) Representative images showing total GFP emission imaged by
987 Typhoon scanning of the 24-well plate.
988